applied sciences

MDPI

Article

Correlation Between Impervious Surface and Surface Temperature Change in Typical Urban Agglomerations—The Case Study of Xuzhou City, China

Yandong Gao, Huiqin Liu *, Hua Zhang, Nanshan Zheng, Shijin Li, Shubi Zhang, Di Zhang, Zhi Li and Chao Yan

School of Environment and Surveying and Mapping, China University of Mining and Technology, Xuzhou 221116, China; ydgao@cumt.edu.cn (Y.G.); zhhua_79@163.com (H.Z.); znshcumt@cumt.edu.cn (N.Z.); shijin_li@cumt.edu.cn (S.L.); zhangsbi@vip.sina.com (S.Z.); liz@cumt.edu.cn (Z.L.); ychao@cumt.edu.cn (C.Y.)
* Correspondence: liuhuiq@cumt.edu.cn

Abstract: Impervious areas are one of the important indicators for evaluating the urbanization process, while surface temperature is one of the reference factors for evaluating the urban environment. In order to investigate whether the spatial distribution of an impervious surface has any influence on urban surface temperature, Xuzhou City was selected as the study area, and the impervious surface information was extracted based on the maximum likelihood classification method for Xuzhou City for the period of 2013–2022, and surface temperature inversion was performed using Landsat 8 remote sensing imagery and nighttime lighting data. In order to reduce the confusion between bare soil and impervious surfaces, the study area was divided into built-up and non-built-up areas for the selection of impervious and pervious surface samples using nighttime lighting data, and, finally, the maximum likelihood classification method was used to realize the extraction of impervious surfaces. The experimental results show that, by extracting the impervious surface of Xuzhou City, the impervious surface of Xuzhou City continued to increase from 2013 to 2022, in which the growth rate was faster in 2014–2016 and 2019–2021, and slower in 2017–2018 and 2021–2022, after performing surface temperature inversion as well as temperature grading. The results of impervious surface extraction and surface temperature inversion were subjected to overlay analysis and linear regression analysis. It was found that most of the impervious surface area is in high-temperature areas, and the density of the impervious surface is proportional to the surface temperature in the impervious surface and its surrounding area. Therefore, it can be concluded that the expansion of impervious surfaces is one of the reasons for the increase in urban surface temperature.

Keywords: impervious surface; land surface temperature; supervision and classification; spatio-temporal variation

check for updates

Citation: Gao, Y.; Liu, H.; Zhang, H.; Zheng, N.; Li, S.; Zhang, S.; Zhang, D.; Li, Z.; Yan, C. Correlation Between Impervious Surface and Surface Temperature Change in Typical Urban Agglomerations—The Case Study of Xuzhou City, China. *Appl. Sci.* **2024**, *14*, 11803. https://doi.org/10.3390/app142411803

Academic Editor: Constantinos A. Balaras

Received: 14 October 2024
Revised: 8 December 2024
Accepted: 13 December 2024
Published: 17 December 2024

Copyright: © 2024 by the authors. Licensee MDPI, Basel, Switzerland. This article is an open access article distributed under the terms and conditions of the Creative Commons Attribution (CC BY) license (https://creativecommons.org/licenses/by/4.0/).

1. Introduction

The periodic monitoring of the urbanization process, ecological changes, and land use patterns is conducive to the sustainable development of urban agglomerations. Impervious surface refers to the surface covered by impermeable materials such as asphalt and cement, usually including roofs, parking lots, roads, and other surfaces with low permeability [1]. Impervious surface area (ISA) is one of the most important indicators for evaluating the degree of urbanization, and impervious surfaces are replacing natural surfaces such as vegetation, farmland, and rivers in the process of large-scale urbanization, which can easily lead to a series of environmental problems [2–4]. With urban development, the urban green area shrinks and the impervious surface expands, leading to a gradual increase in urban surface temperature. This can easily cause the urban heat island effect, so it is important to study the effect of impervious surfaces on surface temperature to predict and control the urban surface temperature [5].

The main methods of impervious surface extraction are the exponential method, spectral mixture analysis, and regression method. The exponential modeling approach is used to extract information about features based on differences in reflections of various features at different ranges by constructing a mathematical model. Some of the widely used exponential models are the P-index, impervious surface area index (ISA), Normalized Impervious Surface Index (NDISI), Modified Normalized Difference Impervious Surface Index (MNDISI), and triple-exponential methods, among others [6–9]. The ISA index can effectively differentiate between vegetated and impervious surfaces, but ignores the effects of soils and water bodies, and has a narrower scope of application, only applying to areas where the cover type is predominantly impervious and vegetated. The NDISI index can more accurately distinguish between different land cover types in urban areas and can better minimize the influence of soil on impervious surface extraction, but the classification accuracy is low [10,11]. The MNDISI index is based on the NDISI index combined with high-resolution nighttime light data to improve the extraction accuracy, but the nighttime light data are difficult to obtain, and the water body needs to be masked before use, which is a complicated process with many processing steps, and its application is limited [12]. Mu Yachao et al. proposed a new Enhanced Impermeable Surface Index (ENDISI), which can effectively eliminate the interference of sandy bare ground in arid areas [13]. The construction of the P-index integrates the Impervious Surface Index, the Index-Based Build-Up Index (IBI), and the inverted impervious surface information, which is extracted with high accuracy, but is difficult to compute and is poorly operationalized [14]. Biophysical Composition Index (BCI), Comprehensive Cumulative Index (CBI), and IBI Construction Index belong to the triple index method, and the problem of confusing information on impervious surfaces using this algorithm still exists, making it difficult to ensure accuracy [15,16]. The index method is simple and easy to compute, and can quickly and accurately extract impervious surfaces, but the index construction process is complicated and has low generalizability; in addition, due to the limitation of spatial resolution, there are mixed pixels in the image, which can easily lead to misclassification of features. Conventional remote sensing classification methods, such as the maximum likelihood classification method, can also be used for impervious surface extraction.

Spectral mixing analysis utilizes a chunking method that allows for the determination of the proportions of the spectral components of different features in the same image element. Ridd et al. proposed a new surface model called the vegetation-impervious-soil (V-I-S) model [17]. The model views the surface as an assemblage of vegetation, impervious surfaces, and soils, and attributes the spectral response of different surface types to the relative proportions of these three components. Based on this idea, Roberts et al. developed and tested the Multiple Endmember Spectral Mixture Analysis (MESMA) [18]. Wu et al. improved the linear spectral decomposition method by dividing the surface into four categories: vegetation, soil, high-albedo features, and low-albedo features, and summing the high-albedo and low-albedo features to obtain the urban distribution in the Columbus area [19]. Spectral mixing analysis solves the problem of mixing pixels on low- and medium-spatial-resolution images to a certain extent, but there are still limitations in this method: the feature types in the city are complex, the spectral heterogeneity of impervious surfaces is strong, and the selection of endpoints is subjective, especially for the selection of endpoints in large areas, which is more difficult. At the same time, there are errors in the decomposition results of different features and coverage in the hybrid image element, which can easily lead to the underestimation of areas with high coverage of impervious surfaces easily using the SMA method, and the overestimation of areas with low coverage [20]. Maximum likelihood classification is a conventional classification method based on probabilistic discriminant rules; for a particular image element in a predetermined N classification training dataset, it needs to calculate the probability that the image element belongs to each class in the dataset, and then attribute this image element to the class with the highest probability among them [21].

In summary, it can be seen that the key to ensuring the accuracy of impervious surface extraction is the ability to distinguish the impervious surface from bare soil. Utilizing the Impervious Surface Index to determine impervious surface areas in densely built-up areas effectively reduces the probability of bare soil being misclassified as an impervious surface. It can effectively ensure the accuracy of impervious surface extraction in the area. The brightness information of nighttime lighting data can directly reflect the location of built-up areas within the study area; therefore, the comprehensive application of nighttime lighting data and remote sensing image data can effectively improve the accuracy of impervious surface extraction [22]. Elvidge et al. established a global impervious surface model based on DMSP-OLS and TM data [23]. Cheng Xi et al. integrated spatial and spectral information from nighttime lights and Landsat TM images to realize the identification of impervious surfaces [24]. Tang Pengfei et al. constructed a feature set by spectral and texture features and then used nighttime lighting information and spectral information to select positive and negative samples of impervious surfaces to complete the extraction of impervious surfaces [25], which effectively reduces the influence of bare soil on the extraction of impervious surfaces.

For this purpose, the luminance information of DMSP-OLS-like data [26] is used to obtain the vector map of built-up areas using the spatio-temporal normalized thresholding method based on pseudo-invariant features. Classification samples of water bodies, vegetation, and bare soil were established in the complete image using the corresponding indices, impervious surface classification samples were established in the built-up area using the Enhanced Impervious Surface Index, and the extraction of impervious surfaces was accomplished using the maximum likelihood classification method. Surface temperature inversion was performed using Landsat8 OLI/TIRS C2L2 imagery and surface temperatures were categorized into high-temperature, sub-high-temperature, medium-temperature, sub-low-temperature, and low-temperature zones based on the mean covariance method. The following analyses were performed to investigate the effect of impervious surfaces on surface temperature: (1) The overlay analysis of the impervious surface extraction results from 2013 to 2022 and the results after surface temperature grading in Xuzhou City showed that more than 50% of the impervious surface area is a high-temperature zone or a sub-high-temperature zone. (2) Based on the density of impervious surfaces, Xuzhou City is divided into three parts: impervious surface aggregation area, permeable surface area, and other impervious surface area. The average temperatures of the above three areas were calculated separately, and it was found that the average temperature was the highest in the impervious surface aggregation area. (3) A certain number of samples were selected in and around the built-up area, and the impervious surface density and average temperature of the selected sample areas were calculated and analyzed by linear regression. The results show that surface temperature and impervious surface density are directly proportional. In conclusion, the increase in impervious surface is one of the reasons for the increase in surface temperature, so the monitoring of impervious surfaces is of great significance for the management of the urban environment.

2. Impervious Surface Extraction Method

Firstly, the built-up area threshold is determined using the spatio-temporal normalized threshold method based on pseudo-invariant features using nighttime lighting data to realize the built-up area extraction. Then, the corresponding index is used to establish the classification samples of water bodies, vegetation, and bare soil, respectively. In the built-up area, the Enhanced Impervious Surface Index is used to establish impervious surface samples, and, finally, the maximum likelihood classification method is used to complete the extraction of impervious surfaces. The advantages of using the above method to complete the extraction of impervious surfaces are as follows: (1) The selected built-up area extraction method can quickly determine the thresholds for subsequent years using linear regression analysis after determining the thresholds for the selected base year, which reduces the influence of human subjective factors and makes the built-up area extraction

results more stable and reliable. (2) Creating classification samples using impervious surfaces, vegetation, water body, and bare soil indices eliminates the need to manually select training samples and allows for the rapid creation of denser training samples. (3) The study area was divided into built-up and non-built-up areas, and impervious surface samples were selected in the built-up areas using the Enhanced Impervious Surface Index (EISI), which effectively reduces the potential for confusion between impervious surfaces and bare soil, improving the separability of impervious surfaces and bare soil. The technology roadmap is shown in Figure 1.

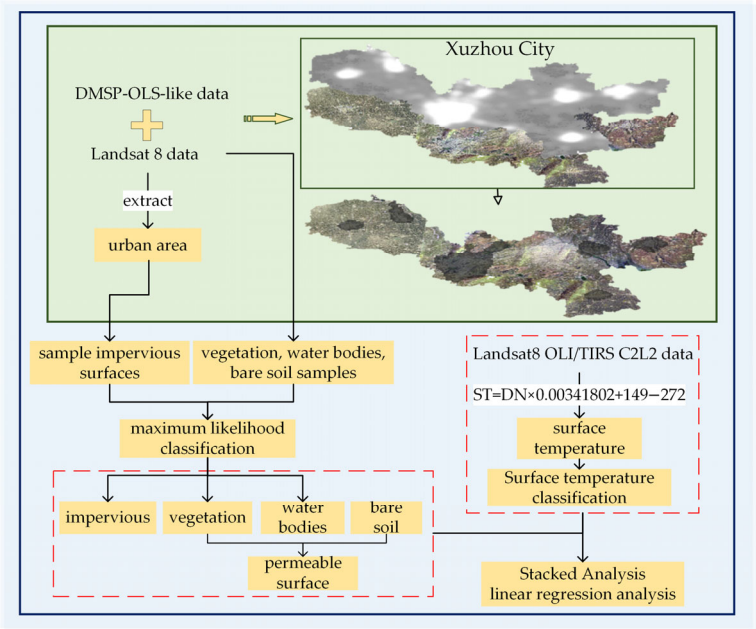


Figure 1. Technology roadmap for impervious surface extraction.

2.1. Extraction of Built-Up Areas

The extraction of built-up areas is accomplished using the integrated and improved DMSP-OLS data using the spatio-temporal normalized thresholding method based on pseudo-invariant features. The method is mainly divided into the following three steps to realize the extraction of built-up areas: (1) Selection of the base year and determination of the optimal threshold for the base year. Using 2013 as the base year, nighttime light imagery and Landsat TM imagery were overlaid to determine an appropriate threshold, and a threshold of 45 was selected for 2013. (2) Determining desaturated pseudo-invariant features. Nighttime light intensity in most urban patches peaks at the city center and gradually decreases from the city center to the periphery of the city; the process of urbanization is irreversible, and it is assumed that these urban areas delineated by the base year will remain urban in the succeeding years. (3) Normalization method for built-up area extraction. A linear regression model was used to relate the *DN* values within the region of desaturated pseudo-invariant features between the reference year and the following year, as shown in Equation (1):

$$DN_t = \alpha + \beta \times DN_0 \quad (1)$$

where DN_0 is the gray value of lights in the reference year, DN_t is the gray value of lights in the desired year, and α and β are the intercept and slope of the linear regression model, respectively. The urban threshold T_0 for the reference year is used to determine the built-up area extraction threshold T_0 for year t through Equation (2).

$$T_t = \alpha + \beta \times T_0 \quad (2)$$

(4) Eliminate outliers. To ensure the reliability of the resulting linear regression equation to eliminate outliers, all the original data are substituted into Formula (2) to obtain the predicted *DN* value, the residuals between the *DN* value and the actual value are calculated, the residuals should obey the normal distribution, the standardized residuals are calculated through Formula (3), and the sample points below the 95% confidence level are eliminated as outliers. The final values are obtained to determine the built-up area extraction thresholds for the study year and to complete the extraction of built-up areas:

$$\delta* = \frac{\delta - \overline{\delta}}{\sigma(\delta)} \tag{3}$$

where δ is the residual between the *DN* value of the predicted value and the actual value, $\sigma(\delta)$ is the standard deviation of δ, and $\delta*$ is the standardized residual.

2.2. Impervious Surface Extraction

Using the Impervious Surface Index and the bare soil index to establish impervious surface and bare soil areas of interest, impervious surfaces and bare soil are easily confused, which seriously affects the accuracy of impervious surface extraction, whereas using the Impervious Surface Index in the impervious surface aggregation area can establish impervious surface samples with high separability. Therefore, the Normalized Vegetation Index (NDVI), Normalized Difference Water Body Index (MNDWI), and Arid Water Body Index (IBAI) were used to establish the vegetation, water body, and bare soil areas of interest. Impervious surfaces are concentrated in the built-up area, and the Enhanced Impervious Surface Index (ENDISI) is used to establish impervious surface interest zones in the built-up area to enhance the separability of the sample pool, and, finally, to realize the extraction of impervious surfaces by using the maximum likelihood classification method. The indices are shown in Equation (4):

$$\begin{cases} NDVI = \frac{B_5 - B_4}{B_5 + B_4} \\ MNDWI = \frac{B_3 - B_6}{B_3 + B_6} \\ IBAI = \frac{(B_5 + B_6) - (B_2 + B_3 + B_4)}{(B_5 + B_6) + (B_2 + B_3 + B_4)} \\ ENDISI = \frac{(2B_2 + B_7)/2 - (B_4 + B_5 + B_7)/3}{(2B_2 + B_7)/2 + (B_4 + B_5 + B_7)/3} \end{cases} \tag{4}$$

where *B2*, *B3*, *B4*, *B5*, *B6*, and *B7* represent the blue, green, red, near-infrared, short-wave infrared1, and short-wave infrared2 of Landsat8 images, respectively. The use of correlation indices to establish areas of interest is more rapid than manual sample selection and allows for the establishment of denser and larger samples. Extracting vegetation using the NDVI index in areas with moderately sparse vegetation and the presence of bare cropland can distinguish soils well. The MNDWI index using green and mid-infrared waves can distinguish buildings and water bodies well. The IBAI index can distinguish bare cropland from impervious surfaces, selecting the ENDISI index to establish the impervious surface area of interest can effectively eliminate the interference of sandy bare land in arid zones, and the use of the appropriate index to establish the area of interest can effectively improve the separability of samples, thus improving the accuracy of impervious surface extraction.

3. Experimental Results and Analysis

3.1. Study Area and Data

Xuzhou is the central city of the Huaihai Economic Zone, and its urbanization development is one of the important indicators of the degree of development of the Huaihai Economic Zone. Xuzhou is located in the southeastern part of the North China Plain, between longitude 116°22′–118°40′ E and latitude 33°43′–34°58′ N, covering an area of 11,765 km^2. Xuzhou City is dominated by plains, which account for more than 90% of the area, with a few hills and mountains in the central and eastern parts of the city, as shown in Figure 2. (The map of China shown here is based on the standard map with review number

GS (2016) 2923 downloaded from the website of the Standard Map Service of the Ministry of Natural Resources, with no modifications to the base map). There is a large amount of farmland distributed in the central part of Xuzhou City, and the confusion between impervious surfaces and bare soil is an urgent problem for impervious surface extraction.

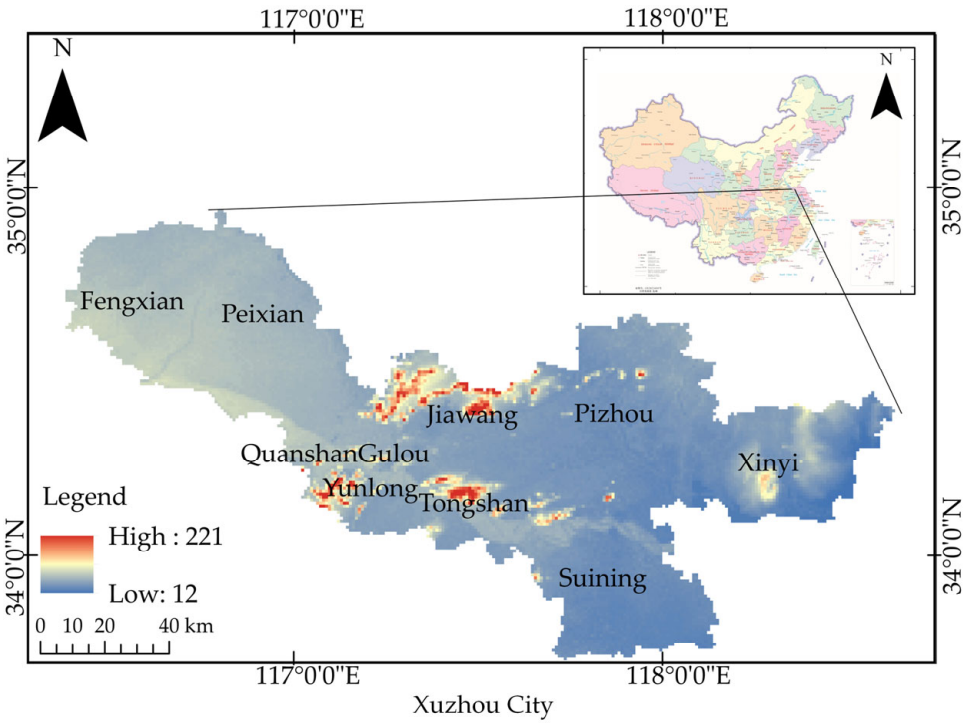


Figure 2. Overview of the study area. (Standard map with review number GS (2016) 2923 downloaded from the website of the Standard Map Service of the Ministry of Natural Resources).

The extraction of built-up areas was completed using the integration of DMSP-OLS-like data. The Landsat8 OLI/TIRS C2L2 remote sensing image data covering Xuzhou City in September and October from 2013 to 2022 were downloaded from USGS, and the overall cloudiness of the study area was ensured to be less than 20% to ensure the extraction accuracy of the impervious surfaces. Tang Pengfei et al. constructed a feature set by spectral and texture features, and then used nighttime lighting information and spectral information to select positive and negative samples of impervious surfaces to complete the extraction of impervious surfaces. The image is spliced and cropped to obtain the image map of Xuzhou City. Landsat8 OLI/TIRS C2L2 10-band images were used to complete the inversion of surface temperature.

3.2. Analysis of Spatial and Temporal Changes in Impervious Surfaces

Figure 3 shows the distribution of impervious areas in Xuzhou City in 2013, 2018, and 2022 (2013–2022 Xuzhou City Impervious Surface Extraction Results in Supplementary Materials), as well as the change in the impervious surface distribution. From Figure 3d, it can be seen that the distribution of impervious areas in the center of Xuzhou City is relatively stable. In order to further analyze the change rule of impervious areas in Xuzhou city from 2013 to 2022, the impervious area of Xuzhou city in each year was calculated and linearly analyzed; as shown in Figure 4, the impervious area of Xuzhou city increased by 637.17 km^2 from 2013 to 2022.

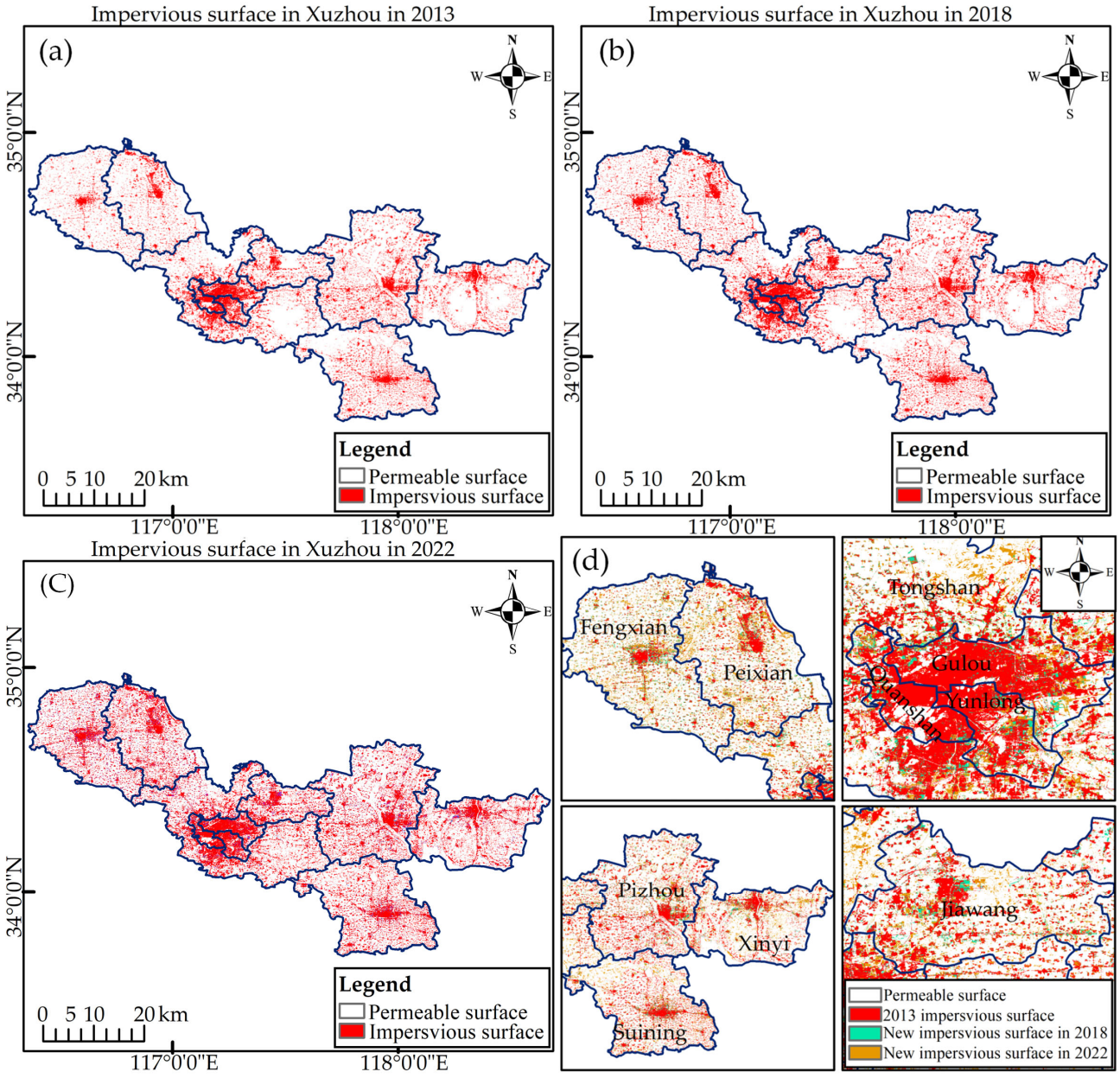


Figure 3. The distribution of impervious surfaces in Xuzhou City from 2013 to 2022. (**a**–**c**) show the impervious area extraction results for Xuzhou City in 2013, 2018 and 2022, respectively. (**d**) Changes in the distribution of impervious surface in some areas of Xuzhou City in 2013, 2018 and 2022.

The change in impervious surfaces was analyzed based on the growth trend of impervious surfaces by dividing it into two phases, 2013–2018 and 2018–2022. During the period of 2013–2018, the growth of impervious surface areas was higher in 2013–2016, with an increase of 101.73 km^2 and 127.86 km^2, respectively; in 2016–2018, the growth rate became slower, increasing by 10.15 km^2 and 9.17 km^2, respectively. In the phase 2018–2022, there was an increase of 86.30 km^2, 102.32 km^2, and 78.79 km^2 in the years 2018–2021, while there was only an increase of 11.69 km^2 in the period 2021–2022. Both phases of impervious surface area change were characterized by a rapid increase in impervious surface followed by stabilization, with a period of plateauing after a period of substantial growth in impervious surfaces. Analyzing the distribution of impervious surfaces in the counties and cities of Xuzhou City from 2013 to mid-2022, it can be found that the distribution of impervious surfaces in the Quanshan District, the Gulou District, and the Yunlong District is the most intensive. More than 30% of the area has impervious surfaces, and Feng County

has the smallest percentage of impervious surfaces, with only about 7% of the area having impervious surfaces. Tongshan District had the largest increase in impervious surfaces, with an increase of 112.74 km^2, and Feng County had the fastest growth rate of impervious surfaces of 94.15 percent, with an increase of 98.99 km^2.

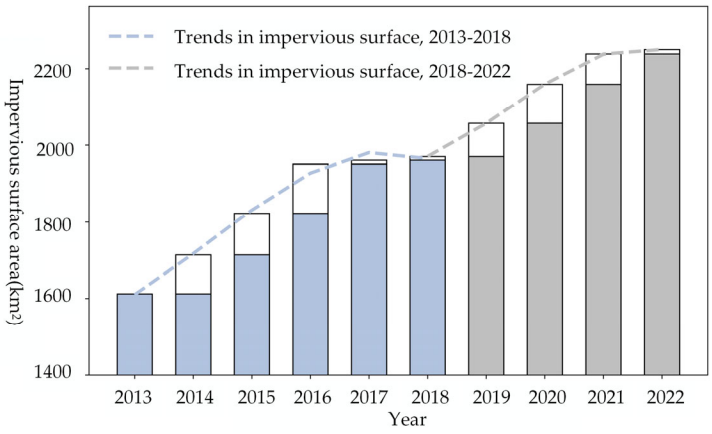


Figure 4. Changes in impervious surface area in Xuzhou City, 2013–2022.

The method accuracy and Kappa coefficient of each type of feature calculated as shown in the confusion matrix can determine whether the classification method used is usable or not. The Kappa coefficient is a metric used for consistency testing, a measure of consistency in statistics with values in the range of $[-1, 1]$, which provides a good measure of the consistency between predicted and actual classification results. In the original image of the study area, 150 sample points were selected, among which 50 sample points were selected for water bodies, vegetation, bare soil, and impervious surfaces, ensuring that the selected sample points were randomly taken and uniformly distributed. The user accuracies were greater than 90% in the years 2013–2022, which demonstrated the reliability of the classification method, and the user accuracies and Kappa of impervious surfaces in the years 2013–2022 are shown in Table 1.

Table 1. Impervious surface extraction accuracy for 2013–2022.

Year	Method Accuracy	Kappa
2013	97.80%	0.8562
2014	97.79%	0.8660
2015	97.81%	0.8851
2016	97.75%	0.8951
2017	97.76%	0.8991
2018	97.77%	0.9025
2019	94.74%	0.8460
2020	92.08%	0.8867
2021	93.23%	0.9109
2022	95.28%	0.9127

3.3. Effect of Impermeable Surfaces on Surface Temperature

The Landsat8 OLI/TIRS C2L2 dataset is a multispectral atmospherically corrected surface reflectance image and surface temperature data, which is a multispectral band surface reflectance and thermal infrared band surface temperature product, and, using the 10th band in the imagery, surface temperatures can be obtained by simple calculations based only on this. The formula is as follows, where DN is the image element value and ST is the surface temperature.

$$ST = DN \times 0.00341802 + 149 - 273 \quad (5)$$

After obtaining the surface temperature using the mean standard deviation method, the surface was divided by temperature into low-, sub-low-, medium-, sub-high-, and high-temperature zones, respectively, and the temperature classes are shown in Table 2. Un is the surface temperature, Um is the mean surface temperature in the study area, and Us is the standard deviation [27].

Table 2. Table of temperature classifications.

Temperature Classification Rules	
Lower temperature	$U_n < U_m - U_s$
Subcooled zone	$U_m - U_s < U_n < U_m - 0.5 \times U_s$
Central temperature area	$U_n - 0.5 \times U_s < U_n < U_m + 0.5 \times U_s$
Subtropical region	$U_m + 0.5 \times U_s < U_n < U_m + U_s$
High-temperature zone	$U_n > U_m + U_s$

To quantitatively analyze the impact of impervious surfaces on surface temperature, the results of temperature classification and impervious surface extraction were overlaid for analysis, and the temperature grading of impervious surface area was obtained, as shown in Table 3, which shows that more than 50% of impervious surfaces in the years 2013–2022 are high-temperature or sub-high-temperature zones. Also, less than 20% of the impervious surface area was in either the cryogenic or sub cryogenic zone from 2013–2022. In contrast, about 50 percent of the permeable surface is distributed in the medium-temperature zone, and about 30 percent is distributed in the low-temperature or sub-low-temperature zone. The temperature in the impermeable surface region is significantly higher than in the permeable surface region.

Table 3. Classification of temperature of impervious surfaces from 2013 to 2022.

Percentage of Impervious Surface Area by Temperature Classification, Xuzhou City, 2013–2018										
	2013	**2014**	**2015**	**2016**	**2017**	**2018**	**2019**	**2020**	**2021**	**2022**
Low temperature	2.2%	1.7%	1.8%	11.4%	7.7%	3.9%	4.5%	3.1%	6.9%	1.6%
Sub-low temperature	3.4%	5.4%	7.0%	6.1%	6.0%	8.0%	4.4%	6.1%	9.4%	3.5%
Medium temperature	33.0%	34.7%	38.7%	22.6%	29.5%	29.0%	29.1%	36.8%	28.9%	34.8%
Sub-high temperature	21.1%	21.2%	22.2%	15.0%	23.0%	21.8%	26.9%	27.3%	17.4%	28.7%
High temperature	40.2%	36.9%	30.0%	44.8%	33.8%	37.3%	35.0%	26.7%	37.5%	31.4%

To visualize the effect of impervious surfaces on the surface temperature, the surface is divided into aggregated impervious surface area, other impervious surface area, and permeable surface area, and the average temperature of each area is calculated; details are shown in Table 4. Aggregated impervious surface areas had the highest average temperatures, followed by other areas of impervious surfaces, and permeable surfaces had the lowest average temperatures. The largest temperature difference was in 2016 when the average temperature in areas with clustered impervious surfaces was 5.49 °C higher than the average temperature on the previous surfaces. This further indicates that the more aggregated the impervious surfaces, the higher the surface temperature.

Figure 5 shows the distribution of impervious surfaces in selected areas in 2013 overlaid with the high-temperature areas from the surface temperature inversion results. From the figure, it can be seen that most of the impervious surface areas are high-temperature zones, especially in the areas where impervious surfaces are aggregated.

Table 4. Average temperature of Xuzhou City from 2013 to 2022.

Zonal Average Temperature 2013–2022 (°C)			
Year	**Impervious Surface Aggregation Zone**	**Other Impervious Surface Areas**	**Permeable Surface Area**
2013	37.11	34.46	32.64
2014	31.90	30.23	28.90
2015	38.54	36.02	34.57
2016	37.34	34.06	31.85
2017	36.13	34.09	32.17
2018	34.30	32.20	30.10
2019	37.30	34.68	31.14
2020	30.58	29.61	27.91
2021	40.23	37.62	35.48
2022	32.60	30.44	28.49

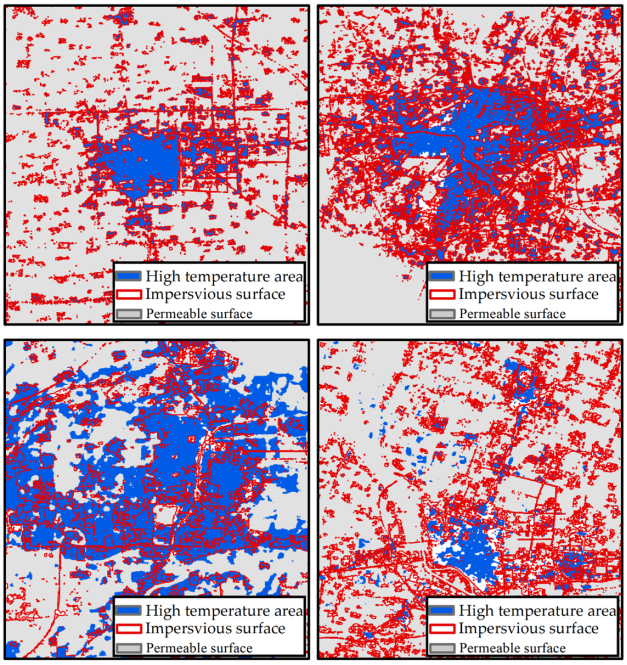


Figure 5. Comparison of temperature classification and impervious surface areas in 2013.

To deeply understand the influence of impervious surfaces on surface temperature, Xuzhou City was randomly divided into 300 blocks and the impervious surface density and average temperature of each block were calculated. The linear regression analysis showed that impervious surface density and surface temperature were positively, but poorly, correlated. It is observed that most of the areas corresponding to outliers are far away from the impervious surface aggregation area and are located in areas with a high percentage of bare soil, where the influence of bare soil on surface temperature is greater than that of impervious surface temperature. In total, 130 sample areas were re-selected in and around the area of impervious surface aggregation, and impervious surface density and average temperature were calculated for each sample. A regression analysis using the percentage of impervious surfaces in the selected blocks as the x-axis and the average temperature as the y-axis revealed that the density of impervious surfaces and the surface temperature are positively correlated. And, the coefficients of determination after removing the outliers were greater than 0.7, which indicated good correlation, and the results are shown in Figure 6. In summary, the increase in impervious surfaces is one of the reasons for the increase in surface temperature.

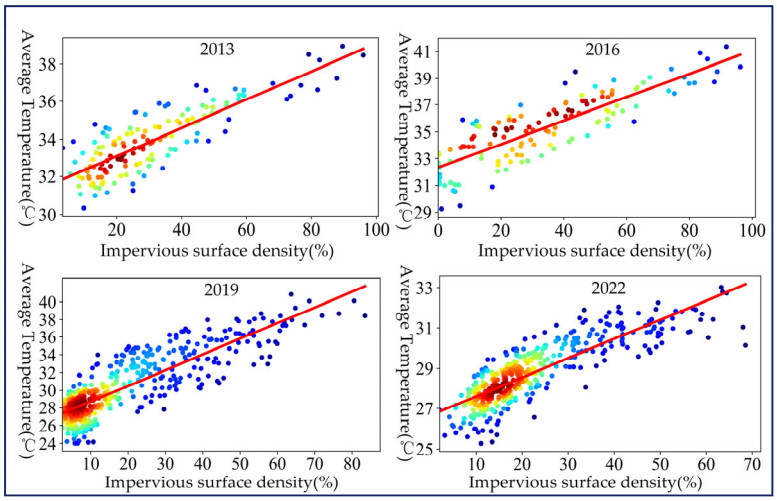


Figure 6. Regression analysis of impermeable surface density and average temperature.

4. Conclusions

The key to ensuring the accuracy of impervious surface extraction is to reduce the confusion between impervious surfaces and bare soil. In the process of realizing the impervious surface extraction in Xuzhou City, the farmland distributed in the middle of Xuzhou City has the greatest influence on impervious surface extraction accuracy. In order to minimize the influence of soil on impervious surface extraction accuracy, Xuzhou City was divided into built-up and non-built-up areas. Only in the built-up area was the Impervious Surface Index used to establish dense and correct impervious surface samples, and supervised classification was used to realize the extraction of impervious surfaces. The final impervious surface extraction accuracy of impervious surfaces is not less than 83.46%, and the Kappa coefficient is not less than 0.85.

(1) Analysis of spatial and temporal changes in impervious surfaces in Xuzhou City. The impervious surface area increased by 637.17 km^2 from 2013 to 2022. The 2014–2016 and 2018–2022 growth rates were faster, and the impervious surface growth rates were similar from 2014 to 2016 with growth rates of 6.33% and 6.37%, and 2018–2021 with growth rates of 4.38%, 4.98%, and 3.65%. The growth became slower in 2017–2018 and 2021–2022, with growth rates of 0.51%, 0.47%, and 0.52%, respectively, increasing by 10.10 km^2, 9.17 km^2, and 11.69 km^2. The distribution of impervious surfaces in Xuzhou City Municipal District City is the most dense, and Feng County has the smallest percentage of impervious surfaces. Tongshan County had the largest increase in impervious surfaces, with an increase of 112.74 km^2, and Feng County had the fastest growth rate of impervious surfaces at 94.15%, with an increase of 98.99 km^2.

(2) Influence of impervious surface distribution on surface temperature in Xuzhou City. From 2013 to 2022, more than 50% of the impervious surface areas in Xuzhou City were either high-temperature or sub-high-temperature zones. Calculating the average temperature by zones, it was found that the temperature in the aggregated impervious surface areas was higher than the temperature in other impervious surface areas, and the average temperature in the permeable surface area was the lowest. Samples were selected in and around impervious surface aggregation areas to calculate their average temperatures and impervious surface densities, regression analyses were performed, and the impervious surface densities were proportional to the average surface temperatures. The increase in impervious surfaces and the decrease in vegetation and bare soil are the inevitable results of urban expansion, but maintaining a favorable urban environment is a prerequisite for ensuring the quality of life of residents. Impervious surfaces are one of the most important factors affecting the surface temperature of the city, so it is important to monitor the temporal and spatial changes in impervious surfaces and the surface temperature of the

city. The timely adjustment of the pace of urban development can reduce the impact of urban development on the environment.

(3) In addition, this paper also has limitations. The selection of impervious and permeable surface samples by thresholding is affected by the spectral texture features of the image as well as the level of visual interpretation. Therefore, further research should be carried out on the method of the automatic acquisition of thresholds in order to improve the accuracy of impervious surface extraction. Meanwhile, the surface temperature is affected by many aspects, such as vegetation rate and elevation. In this paper, there is a limitation that only the impervious surface aggregation area and its surrounding areas are included in the study area. The influence of various factors should be considered in future research.

Supplementary Materials: The following supporting information can be downloaded at: https://www.mdpi.com/article/10.3390/app142411803/s1, File S1. Map of Impervious Surface Extraction Results for Xuzhou City, 2013–2023.

Author Contributions: Conceptualization, Y.G. and H.L.; methodology, Y.G.; software, H.Z.; validation, Y.G., H.L., and H.Z.; formal analysis, H.L.; investigation, S.L.; resources, S.Z.; data curation, N.Z.; writing—original draft preparation, H.L.; writing—review and editing, Y.G.; visualization, Z.L. and D.Z.; supervision, N.Z.; project administration, C.Y.; funding acquisition, Y.G. All authors have read and agreed to the published version of the manuscript.

Funding: This research was funded by the Fundamental Research Funds for the Central Universities, grant number 2023QN1045. This work was supported in part by the National Natural Science Foundation of China under Grant U22A20569.

Institutional Review Board Statement: Not applicable.

Informed Consent Statement: Not applicable.

Data Availability Statement: The raw data supporting the conclusions of this article will be made available by the authors on request.

Conflicts of Interest: The authors declare no conflict of interest.

References

1. Arnold, C.L., Jr.; Gibbons, C.J. Impervious surface coverage: The emergence of a key environmental indicator. *J. Am. Plan. Assoc.* **1996**, *62*, 243–258. [CrossRef]
2. Weng, Q. Remote sensing of impervious surfaces in the urban areas: Requirements, methods, and trends. *Remote Sens. Environ.* **2012**, *117*, 34–49. [CrossRef]
3. Shahtahmassebi, A.R.; Song, J.; Zheng, Q.; Blackburn, G.A.; Wang, K.; Huang, L.Y.; Pan, Y.; Moore, N.; Shahtahmassebi, G.; Haghighi, R.S.; et al. Remote sensing of impervious surface growth: A framework for quantifying urban expansion and re-densification mechanisms. *Int. J. Appl. Earth Obs. Geoinf.* **2016**, *46*, 94–112. [CrossRef]
4. Dutta, D.; Rahman, A.; Kundu, A. Growth of Dehradun city: An application of linear spectral unmixing (LSU) technique using multi-temporal landsat satellite data sets. *Remote Sens. Appl. Soc. Environ.* **2015**, *1*, 98–111. [CrossRef]
5. Li, D.; Liao, W.; Rigden, A.J.; Liu, X.; Wang, D.; Malyshev, S.; Shevliakova, E. Urban heat island: Aerodynamics or imperviousness? *Sci. Adv.* **2019**, *5*, eaau4299. [CrossRef]
6. Carlson, T.N.; Arthur, S.T. The impact of land use—Land cover changes due to urbanization on surface microclimate and hydrology: A satellite perspective. *Glob. Planet. Chang.* **2000**, *25*, 49–65. [CrossRef]
7. Xu, H. Analysis of impervious surface and its impact on urban heat environment using the normalized difference impervious surface index (NDISI). *Photogramm. Eng. Remote Sens.* **2010**, *76*, 557–565. [CrossRef]
8. Liu, C.; Shao, Z.; Chen, M.; Luo, H. MNDISI: A multi-source composition index for impervious surface area estimation at the individual city scale. *Remote Sens. Lett.* **2013**, *4*, 803–812. [CrossRef]
9. Xu, H. A new index for delineating built-up land features in satellite imagery. *Int. J. Remote Sens.* **2008**, *29*, 4269–4276. [CrossRef]
10. Xu, H.Q.; Wang, M.Y. Analysis of Main Remote Sensing Methods for Surface Impermeable Water Surface Information. *J. Remote Sens.* **2016**, *20*, 1270–1289.
11. Bektaş Balçik, F. Determining the impact of urban components on land surface temperature of Istanbul by using remote sensing indices. *Environ. Monit. Assess.* **2014**, *186*, 859–872. [CrossRef] [PubMed]
12. Wang, Z.; Gang, C.; Li, X.; Chen, Y.; Li, J. Application of a normalized difference impervious index (NDII) to extract urban impervious surface features based on Landsat TM images. *Int. J. Remote Sens.* **2015**, *36*, 1055–1069. [CrossRef]
13. Mu, Y.C.; Ling, Y.W.; Zhang, L.L.; Chen, Y.H. A New Enhanced Impermeable Surface Index. *Sci. Surv. Mapp.* **2018**, *43*, 83–87.

14. Ma, Y.; Kuang, Y.; Huang, N. Coupling urbanization analyses for studying urban thermal environment and its interplay with biophysical parameters based on TM/ETM+ imagery. *Int. J. Appl. Earth Obs. Geoinf.* **2010**, *12*, 110–118. [CrossRef]
15. Deng, C.; Wu, C. BCI: A biophysical composition index for remote sensing of urban environments. *Remote Sens. Environ.* **2012**, *127*, 247–259. [CrossRef]
16. Sun, G.; Chen, X.; Jia, X.; Yao, Y.; Wang, Z. Combinational build-up index (CBI) for effective impervious surface mapping in urban areas. *IEEE J. Sel. Top. Appl. Earth Obs. Remote Sens.* **2015**, *9*, 2081–2092. [CrossRef]
17. Ridd, M.K. Exploring a VIS (vegetation-impervious surface-soil) model for urban ecosystem analysis through remote sensing: Comparative anatomy for cities. *Int. J. Remote Sens.* **1995**, *16*, 2165–2185. [CrossRef]
18. Roberts, D.A.; Gardner, M.; Church, R.; Ustin, S.; Scheer, G.; Green, R.O. Mapping chaparral in the Santa Monica Mountains using multiple endmember spectral mixture models. *Remote Sens. Environ.* **1998**, *65*, 267–279. [CrossRef]
19. Wu, C.; Murray, A.T. Estimating impervious surface distribution by spectral mixture analysis. *Remote Sens. Environ.* **2003**, *84*, 493–505. [CrossRef]
20. Lu, D.; Weng, Q.; Li, G. Residential population estimation using a remote sensing derived impervious surface approach. *Int. J. Remote Sens.* **2006**, *27*, 3553–3570. [CrossRef]
21. Jensen, J.R. *Introductory Digital Image Processing, A Remote Sensing Perspective*, 4th ed.; Pearson Prentice Hall: Saddle River, NJ, USA, 2015.
22. Sutton, P.; Roberts, D.; Elvidge, C.; Baugh, K. Census from Heaven, An estimate of the global human population using night-time satellite imagery. *Int. J. Remote Sens.* **2001**, *22*, 3061–3076. [CrossRef]
23. Elvidge, C.D.; Tuttle, B.T.; Sutton, P.S.; Baugh, K.E.; Howard, A.T.; Milesi, C.; Bhaduri, B.L.; Nemani, R. Global distribution and density of constructed impervious surfaces. *Sensors* **2007**, *7*, 1962–1979. [CrossRef] [PubMed]
24. Cheng, X.; Wu, W.; Xia, L.G.; Luo, R.; Shen, Z.F. Research on Automatic Extraction of Impermeable Surface by Integrating Nighttime Light Data and Landsat TM Images. *J. Earth Inf. Sci.* **2017**, *19*, 1364–1374.
25. Tang, P.F.; Miao, Z.M.; Lin, C.; Du, F.J.; Guo, S.C. An Automatic Extraction Method for Impermeable Surface by Integrating High Resolution Night Light and Landsat OLI Images. *J. Infrared Millim. Waves* **2020**, *39*, 128–136.
26. Wu, Y.; Shi, K.; Chen, Z.; Liu, S.; Chang, Z. Developing improved time-series DMSP-OLS-like data (1992–2019) in China by integrating DMSP-OLS and SNPP-VIIRS. *IEEE Trans. Geosci. Remote Sens.* **2021**, *60*, 4407714. [CrossRef]
27. Zhang, J. *Remote Sensing and Spatial and Temporal Evolution of Surface Thermal Environment in the Pearl River Delta Region*; Guangzhou Institute of Geochemistry, Chinese Academy of Sciences: Guangzhou, China, 2006.

Disclaimer/Publisher's Note: The statements, opinions and data contained in all publications are solely those of the individual author(s) and contributor(s) and not of MDPI and/or the editor(s). MDPI and/or the editor(s) disclaim responsibility for any injury to people or property resulting from any ideas, methods, instructions or products referred to in the content.